Carbon Resources Conversion 5 (2022) 71–83

Contents lists available at ScienceDirect

Carbon Resources Conversion

journal homepage: www.keaipublishing.com/en/journals/carbon-resources-conversion

Model of an iron ore sinter plant with selective waste gas recirculation

Johannes Niel [a,*], Bernd Weiss [b], Walter Wukovits [a]

[a] TU Wien, Institute of Chemical, Environmental and Bioscience Engineering, Getreidemarkt 9/166, 1060 Vienna, Austria
[b] Primetals, Primetals Technologies Austria GmbH, Linz, Austria

ABSTRACT

The use of sinter influences hot metal production substantially and significantly affects an integrated steel mill's total emissions. Sintering of iron ores is an enormous energy-intensive and resources consuming process. Introducing a selective waste gas recirculation (SWGR) to the sintering process reduces the energy consumption, stack gas volume flow, and sulfur dioxide emissions of an iron sinter production. Simulating this complex process in flowsheet simulations of integrated iron and steelworks is a fast and cost-effective opportunity to validate new operation settings. The implementation of a sinter plant in gPROMS ModelBuilder®characterizes the sintering processes by three main sub-models. A burner model describes the gas combustion, a black-box model consider the main sintering processes, and a wind box model divides the total off-gas into a recycle gas and a stack gas. A specific temperature polynomial represents the temperature distribution across the wind boxes to allow detailed investigations on SWGR in complex flowsheet simulations. Implementing SWGR to the sintering process, the model shows a reduction of coke consumption, stack gas flow rate, and sulfur dioxide emissions by 11%, 27%, and 27%, respectively. In the SWGR scenario, the utilization rate of carbon monoxide increases and less coke is consumed. The chlorine emissions of the sintering process differ with and without SWGR insignificantly.

1. Introduction

Using sinter as feedstock for the burden has many positive effects on the blast furnace process. The advantages of an iron ore sinter are its high porosity, adjustable chemical composition, constant melting behavior, and stable mechanical properties. Therefore, the use of sinter increases the efficiency of hot metal production. Fines cannot be used directly for the burden due to their lightweights and negative influence on the blast furnace process. (e.g., increasing pressure drop). With iron ore sintering, iron fines are utilizable for pig iron production. The sintering process is influenced extensively by the properties of the input material and process conditions. The operating setting essentially influences the properties of the sintered product [1].

1.1. Sinter Plant Process

Solid input for the sintering process comprises iron carrier (e.g., iron ores), additives (e.g., limestone, dolomite, burned lime), and fuels (e.g., coke breeze, coal). The gaseous input includes air, and gaseous fuels (e.g., natural gas, blast furnace gas) [1].

Fig. 1 illustrates the general sinter process scheme. In the first step of the sintering process, raw materials are mixed in a rotary drum. Water is added to achieve a homogeneous particle size through agglomeration in the granulator. In the next step, the raw mixture is placed on moving pallet cars. Under the ignition hood, the sintering reaction is started on the top of the sinter bed. Blowers, which are located under the sinter strand, suck gas through the sinter bed. The sintering reaction is moving to the bottom of the sinter bed. At the end of the sinter strand, the produced sinter is crushed, cooled, and sieved into three fractions. The sinter fines, which are the first fraction, are recirculated to the proportioning bins, the second fraction is used as the heart layer on the pallet cars, and the third fraction is the sintered product to be used in the blast furnace [2].

Wind boxes collect the entire off-gas stream underneath the sinter strand, which varies over the total sinter plant length on its volume flow, composition, and temperature. Selective waste gas recirculation (SWGR) of single wind box flowings to the sinter conveyor hood reduces fuel consumption, emissions, and the volume of stack gas [3].

1.2. Sintering Reactions

The sintering process can be described by four zones: 1) A sintered zone (top) for describing the heat exchange between gas phase and solid phase of the sintered material, 2) a reaction zone involving chemical reactions, solidification, and porosity changes, 3) a decomposition zone including thermal decomposition of carbonates, and 4) a raw mix zone (bottom) considering the heat exchange of the solid material and condensation of water.

Once the sintering process has started under the ignition hood, the zones move from top to bottom along the sinter strand's length, as shown in Fig. 2 a. As the sintering proceeds along the sinter strand, the sintered zone is on top of the sinter bed. In this zone, entering process

* Corresponding author.

https://doi.org/10.1016/j.crcon.2022.01.001
Received 2 June 2021; Received in revised form 9 January 2022; Accepted 14 January 2022
Available online 24 January 2022

gas comes into contact with the sintered product. Process gas consists of fresh air, and, in the case of introduced SWGR, a recycled off-gas stream. Because of the heat exchange between the solid and gas phases, the process gas is preheated and the solid material is continuously cooled. At the border to the combustion zone, the sinter solidifies [1,5].

In the combustion zone, the preheated gas stream reacts with carbon by combustion. It is the most exothermic reaction of the sintering process. Due to temperatures above 1100°C, solids are melting without reaching the point of liquefaction. Iron ores are reacting with oxygen. With the chemical conversion of carbon to carbon monoxide and carbon dioxide, the gas volume extends. The porosity of the sinter bed changes significantly [6,5].

The hot gas from the carbon combustion preheats the sinter bed continuously. In the decomposition zone, within the temperature range of 350°C and 1100°C, carbonates (e.g., $CaCO_3, MgCO_3, MnCO_3, FeCO_3$) thermally decompose and released carbon dioxide increases the gas flow. Due to the endothermic decomposition process, the gas flow cools down [2,7–11].

Underneath the decomposition zone, the raw mixture zone is appended. With increasing distance to the combustion zone, temperatures of solids and gases decline. At the point where water is left in the raw mixture, an interaction between the evaporation of water and the partial condensation of the water vapour is formed. During this interaction, the gas temperature remains almost constant and is ranging between 50°C and 70°C. Further cooling occurs along the saturation line depending on the pressure [1,6,12–14].

Due to the above-described drying process of the raw sinter mix in the first half of the sinter strand, off-gas temperatures at first wind boxes range between 50°C to 70°C. Later, when the combustion zone moves to the bottom of the sinter strand, the off-gas temperature increases. When the burning-through-point is reached on the sinter bed bottom, the combustion zone is completed; only the sintered zone is present on the strand. The off-gas temperature declines. The changing conditions on the sinter bed bottom over the sinter length influence the temperature and create changing compositions in the off-gas stream. Fig. 3 shows a typically measured temperature profile over the sinter strand length [1,6,12,13].

Several authors summarized the reaction zone and the decomposition zone to a combustion zone (Fig. 2 b). All considered chemical reactions of the sintering process are occurring in this zone [6,13,15,16].

1.3. Sinter Models

Depending on the sintering process inside the sinter bed, gas flow, composition, and temperature change. Unsteady 1D sinter models are commonly used to describe the sintering process. Muchi and Higuchi developed one of the first computed sinter models. The focus was mainly on the coke combustion but they also considered the water load, the sintering speed, diffusion of oxygen, and carbon dioxide in the gas phase, and the particle diameter [17].

Another one-dimensional sinter model was developed by Mitterlehner et al. They mainly focused on describing the propagation velocity of the heat front inside the sinter bed. The model considers a description of the gas flow in the sinter bed, a heterogeneous catalyzed oxidation of carbon monoxide, thermal decomposition of carbonates, and the partial melting and solidifying processes of the solids [7].

Yang et al. developed a one-dimensional model which considers multiple solid phases, heat transfer between the solid phases, radiative heat transfer, changes of the bed structure based on particle size changes, and the main sintering reactions (vaporization/condensation of water, coke combustion, and limestone decomposition) [16].

Nath et al. developed a two-dimensional model, considering heat

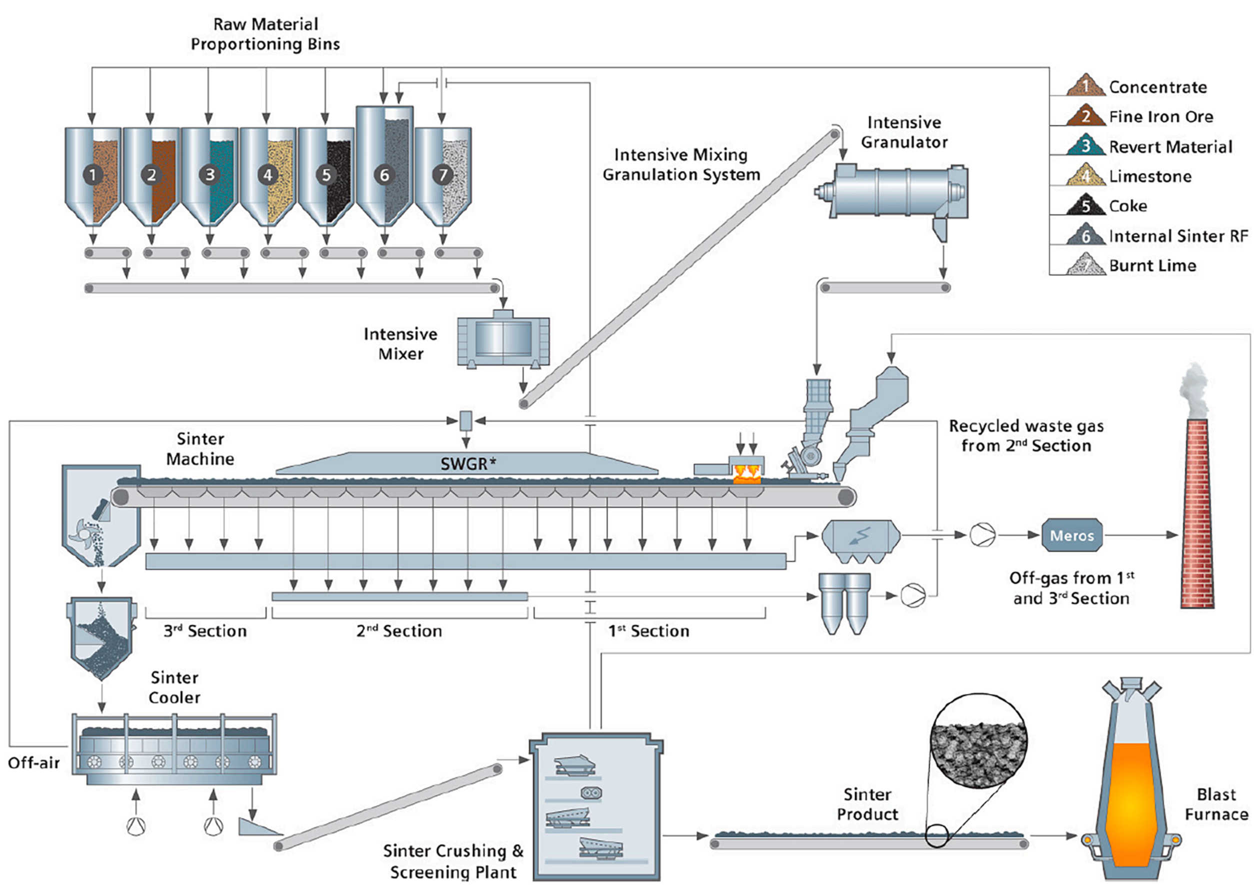

Fig. 1. Schematic overview of the sintering process [4].

propagation and sinter productivity [13]. De Castro developed a three-dimensional sinter model and investigated influences of different gas compositions and their effects on off-gas emissions [18,19]. Ramos et al. tried to predict melting and molten zone more precisely in the sinter bed via DEM simulation [20].

Zhang et al. worked on a 1D model that considers a selective waste gas recirculation (SWGR). They investigated the influence of SWGR on the sinter productivity and sinter quality and defined essential parameters of the recycle gas. The most crucial factor is the oxygen content in the process gas, which should be between 19–20 percent. Other essential parameters are the amount and temperature of the recycled gas [21]. Over the last ten years, investigations on gaseous fuel injections have been done. Such an injection creates a secondary combustion zone above the solid fuels combustion zone, enabling an increased sinter strength with lower solid fuel consumption and influences the vapor content in the off gas [22–25]. With growing interest in this topic, sinter models considering gaseous fuel injection are developed. Ni et al. investigated the influence of coke oven gas injection on specific positions of the sinter strand and validated the simulation results with sinter pot tests [26]. Tsioutsios et al. developed a non-stationary 1D model for parameter studies for supporting sinter pot experiments. This model demonstrates that coke can be moderately reduced with pulsed gaseous fuel injection without reducing the sinter strength [27].

These detailed sintering models give detailed insight in the sintering process, enabling investigations of effects difficult to measure. Due to the time consuming calculations, detailed simulation models are hardly applicable to flowsheeting simulations of complete iron and steel production plants. For this purpose Rentz et al. developed a sinter plant model in Aspen Plus®, based on a 3x3 reactor matrix describing the sinter bed. In the matrix-diagonal, chemical equilibrium reactors (RGIBBS) are positioned to specify the combustion zone. The reactors which are located above the matrix-diagonal, characterize the progress of the sintered zone, reactors under the matrix-diagonal describe the progress of the raw mix zone [15]. Ahn et al. developed a sinter strand model in Aspen Plus ®, which is similar to the Rentz et al. model. The difference is that Ahn discretized the sinter bed by a 14x14 reactor-matrix, and only in the matrix-diagonal RGIBBS reactors are used. The other reactors are yield or flash reactors. Both models require predefined reactor temperatures. Based on the chemical reactor design, the temperature profile of the off-gas stream over the total sinter strand length is assigned at the beginning of the simulation [6].

1.4. Motivation

The challenge of describing the general sintering process is its complexity since different process steps are linked. Carbon combustion, thermal decomposition, water vaporization, and condensation influence the sinter bed's temperature, melting and solidification behavior, pressure drop due to porosity and temperature changes, gas and solid compositions, and the sinter quality, and productivity. Most of the caused process and material alterations significantly affect the chemical reaction in the sinter bed. Detailed sinter models consider these effects in time-consuming calculations.

The prerequisites for a useful application of a process simulation model are that it should be time-saving and comprise only a small number of fitting parameters.

Due to the time-saving focus, models from Rentz et al. and Ahn et al. are an attractive option. Nevertheless, a significant drawback of these

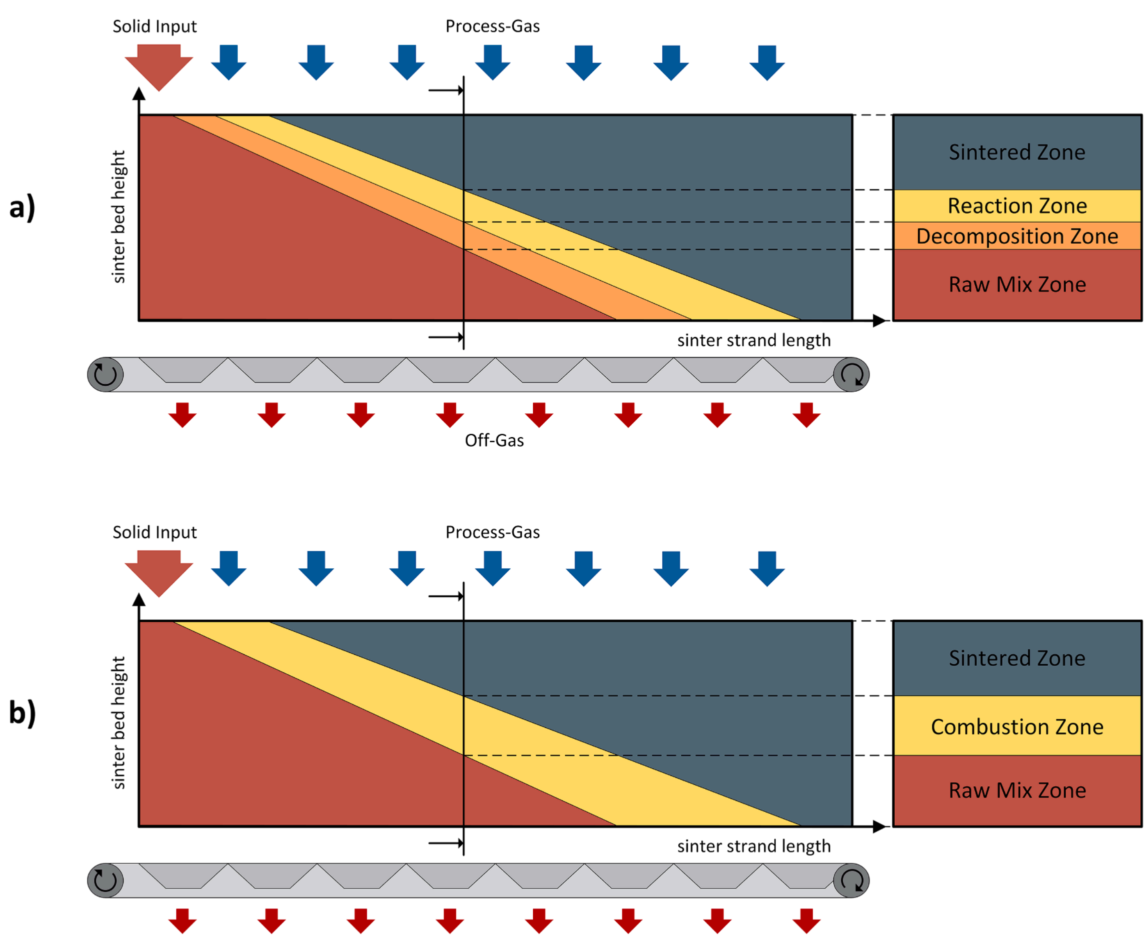

Fig. 2. Scheme of sintering zones inside the sintering bed.

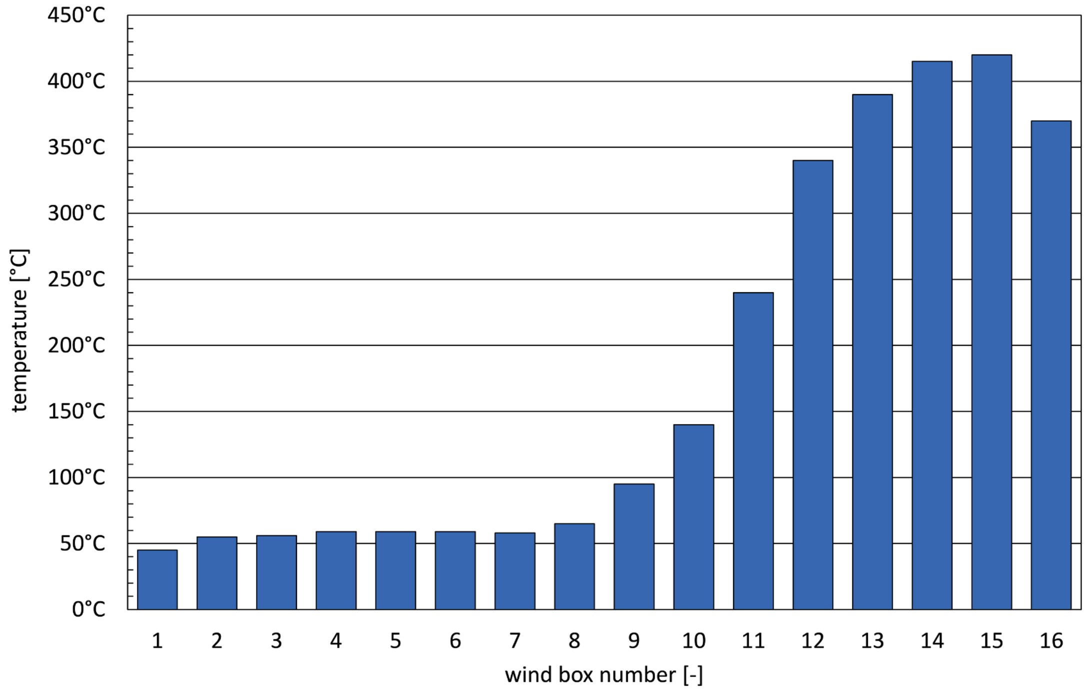

Fig. 3. Typical temperature distribution of a sinter strand [1].

models is the necessary assignment of the reactor temperature or a to each RGIBBS Model. Nevertheless, a significant drawback of these models is the calibration of the reactor temperatures and the consideration of deviations from chemical equilibrium with empirical parameters.Therefore, the each reactor temperatures must be carefully calibrated for each new simulation scenario.

A model that combines physical relations and empirical approaches to temperature behavior and material flows enables short-time simulations and reduces the number of calibration parameters. This model-design is applicable for foreward and backward calculations and enables advanced flowsheet simulations of highly integrated steelworks. Simplifications do not allow a detailed description of the sintering process or sinter properties, but allow - with valid boundaries - a global investigation on the influences of the sintering progress on iron and steel production by focusing on material consumption, environmental impacts, cost efficiencies, operating conditions, and plant geometries are possible.

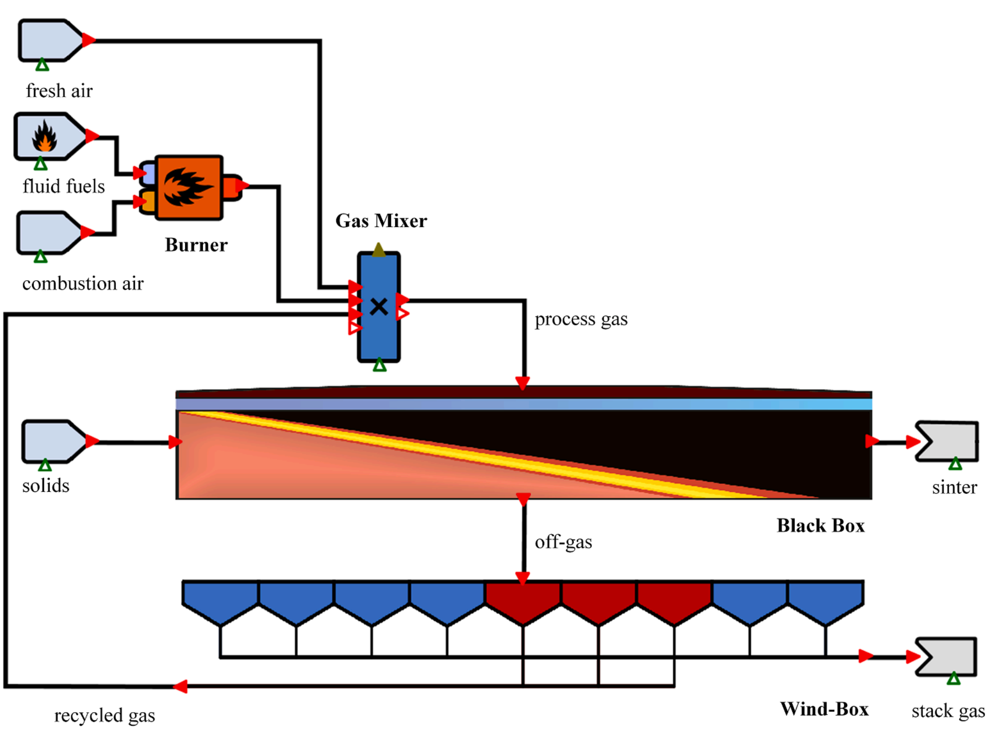

Fig. 4. Schematic of sinter plant model structure.

2. Sinter Model

The sinter plant model developed in gPROMS ModelBuilder® (6.0.4, Process Systems Enterprise limited, December 2019) characterizes main process effects based on three sub-models combining physio-chemical correlations with empirical correlations to minimize parametization of the model for calculation of mass and energy balances of the sintering process. A burner model calculates the combustion gas's composition and the amount of combustion air under adiabatic conditions. A black-box model describes the general sintering process, including main chemical reactions, gas–solid separation, mass and energy balances. A wind-box model calculates each wind box's gas flow and gas temperature based on empirical distribution functions and splits the off-gas flow from the wind boxes into a stack-gas stream, and a recycle stream. Fig. 4 shows a schematic illustration of the sinter plant model.

2.1. Burner Model

The fundamentals of the burner model are based on the assumptions of Beahr and Kabelac [28]. The air to fuel equivalence ratio λ defines the amount of combustion air (Eq. 1). $\dot{m}_{air}$ is the mass flow of total air, $\dot{m}_{air,stoich}$ is the mass flow of air under stoichiometric conditions, and $x_{O_2,air}$ and $x_{O_2,stoich}$ are the content of oxygen under real and stoichiometric conditions, respectively.

$$\lambda = \frac{\dot{m}_{air} \cdot x_{O_2,air}}{\dot{m}_{air,stoich} \cdot x_{O_2,stoich}} \tag{1}$$

$$\sum_{in}(\dot{m}_{in} \cdot \frac{x_{in,k}}{MW_k} \cdot RD) = \sum_{out}(\dot{m}_{out} \cdot \frac{x_{out,k}}{MW_k}) \tag{2}$$

$$\sum_{in}(\dot{m}_{in} \cdot x_{in,k} \cdot h_k(T)) = \sum_{out}(\dot{m}_{out} \cdot x_{out,k} \cdot h_k(T)) + \dot{H}_{losses} \tag{3}$$

Eq. 2 describes the chemical conversions of each gaseous fuel (CO, $C_xH_{y,(g)}$)) with the reaction degree RD. The reaction degree describes the stoichiometric conversion of each chemical reaction. $\dot{m}$ is the mass flow, x is the mass-based composition, and MW is the molecular weight. The index k stands for the chemical component k, *in* for all input streams, and *out* for the output stream. Based on the enthalpy balance Eq. 3, the adiabatic flame temperature is calculated. Non-adiabatic conditions are considered by the enthalpy losses H_{losses}. h(T) is the specific enthalpy at temperature T.

2.2. Black-Box Model

In the black-box model, mass balance and enthalpy balance (Eq. 2–3) are applied along with the stoichiometry of the sinter reactions [4]. Table 1 shows the considered chemical reactions of the black-box model including thermal decomposition of carbonates, carbon combustion, water vaporization, and reactions with alkali and sulfur. The high number of iron reactions during the sintering process causes different handling with iron components. The black-box model includes composition assignments of iron for the sintered material and considers components Fe, FeO, Fe_2O_3, and Fe_3O_4. The oxygen demand for iron oxidation is also considered with an included element balance. The oxygen demand for iron oxidation is also considered with an included element balance. Besides sulfur oxidation, increased sulfur binding in the sinter is observed in scenarios with SWGR (following Schmid et al. [29]). The model considers this behaviour with the back reaction of sulfur dioxide to sulfur, including an empirical conversion factor.

Table 1
Chemical reactions

carbon gasification		water vaporisation
$C + \frac{1}{2}O_2 \rightarrow CO_2$		$H_2O_{(l)} \rightarrow H_2O_{(g)}$
$C + O_2 \rightarrow CO_2$		$Fe_2O_3 \cdot H_2O \rightarrow Fe_2O_3 + H_2O_{(g)}$
CO combustion		**chlorine binding**
$CO + \frac{1}{2}O_2 \rightarrow CO_2$		$\frac{1}{2}H_2 + \frac{1}{2}Cl_2 \rightarrow HCl$
CO_2 release		**alkaline metal oxidation**
$MgCO_3 \rightarrow MgO + CO_2$		$2K + \frac{1}{2}O_2 \rightarrow K_2O$
$CaCO_3 \rightarrow CaO + CO_2$		$2Na + \frac{1}{2}O_2 \rightarrow Na_2O$
$FeCO_3 \rightarrow FeO + CO_2$		
	sulfur reaction	
$S_{(s)} + O_2 \rightarrow SO_2$		$SO_2 \rightarrow S_{(s)} + O_2$

2.3. Wind Box Model

The wind box model splits the off-gas stream into an SWGR stream and a stack gas flow. A wind box flow selector defines both streams by selecting each wind box stream to the stack-gas or SWGR stream. The properties of each wind box flow are defined by component and temperature distributions, thereby reducing the required input parameters while ensuring mass and enthalpy balances. In the following subsections, the methods for calculating mass flow in the wind boxes, and wind box temperatures are described.

2.3.1. Component Distribution

Based on the published concentration of chlorine and sulfur dioxide in wind boxes, polynomials describe the component distributions in the wind box model [30]. Each distribution is regressed based on dimensionless length (Eq. 4). For each simulation scenario, the number of wind boxes can be assigned individually. Therefore the discretization of the distribution function will change.

$$\frac{\dot{m}_j(l_i)}{\dot{m}_{j,total}} = \frac{a_j \cdot l_i^4 + b_j \cdot l_i^3 + c_j \cdot l_i^2 + d_j \cdot l_i + e_j}{\sum_{i=1}^{n} a_j \cdot l_i^4 + b_j \cdot l_i^3 + c_j \cdot l_i^2 + d_j \cdot l_i + e_j} \tag{4}$$

In Eq. 4, j is the index for components and i for the wind box number, a, b, c, d, and e are the regression coefficients, l_i denotes the dimensionless position of wind box i, and $m_{j,total}$ is the total amount of component j in the off-gas stream. This equation design enables simulations for different plant geometries. Component and mass distribution can be used for a feed-forward and feed-backward oriented calculation. Fig. 5 shows the implemented distribution functions of sulfur and chlorine as an example.

2.3.2. Temperature Distribution

Following Eq. 5, the temperature calculation of each wind box T(i) considers the off-gas temperature $T_{off-gas,BB}$ from the black-box model ($T_{off-gas,BB} = T_{inlet,WB}$). $T_{inlet,WB}$ is multiplied with an explicit weighting term. This term includes the regressed function $T_{poly}(i)$, which takes into account the characteristic shape of the temperature distribution over the length of a sintering plant based on observed sensor data, and $T_{leveling}$, a fitting parameter, to ensure a closed enthalpy balance.

$$T(i) = T_{\text{inlet,WB}} \cdot \frac{T_{\text{poly}}(i)}{T_{\text{leveling}}} \tag{5}$$

Fig. 6 shows the calculation of the wind box temperature schematically based on the publication of Cappel and Wendedorn [1]. In this case $T_{inlet,WB}$ equals 150°C and on the secondary axis the deviation of each wind box temperature to T_{inlet} is shown. The deviation is described by the term $T_{poly(x_i)}/T_{leveling}$.

3. Results and Discussion

To demonstrate that the model can describe effects connected with introducing a SWGR and estimating the reduction in coke demand and emissions, the sinter plant model was applied to two different scenarios:

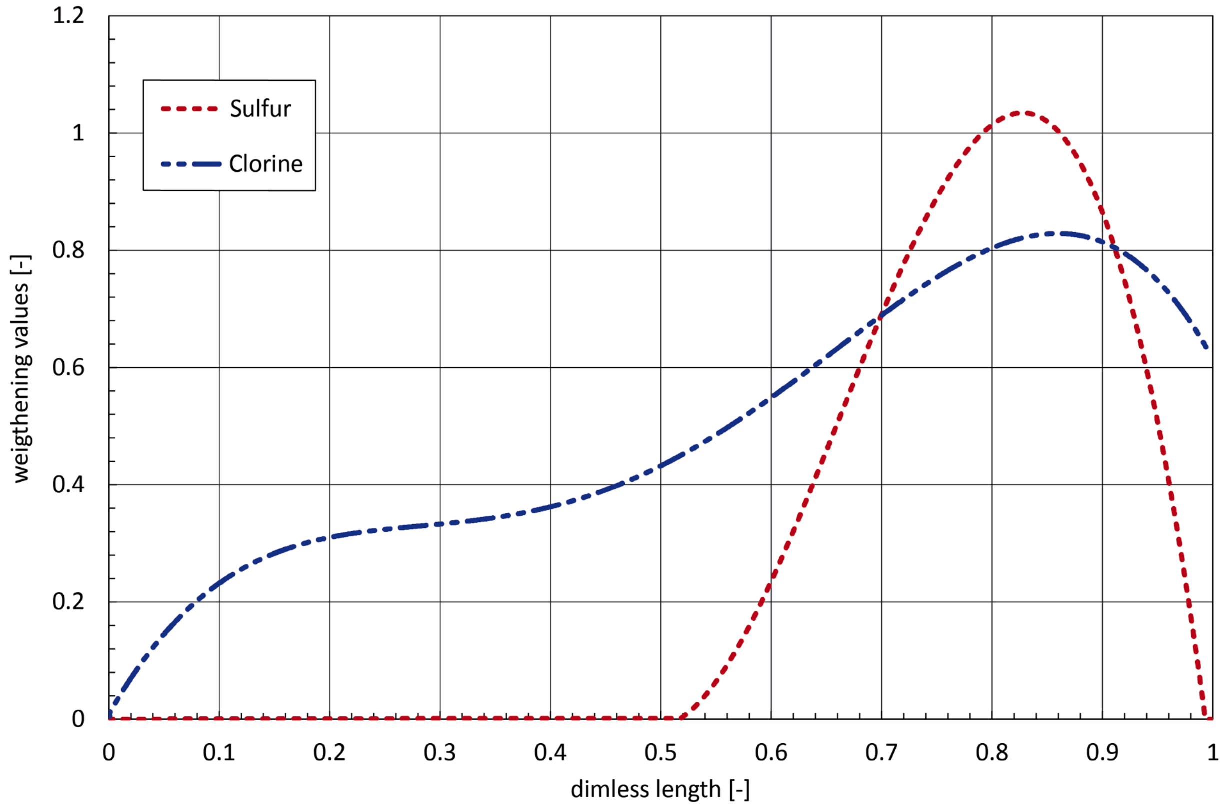

Fig. 5. Implemented distribution functions.

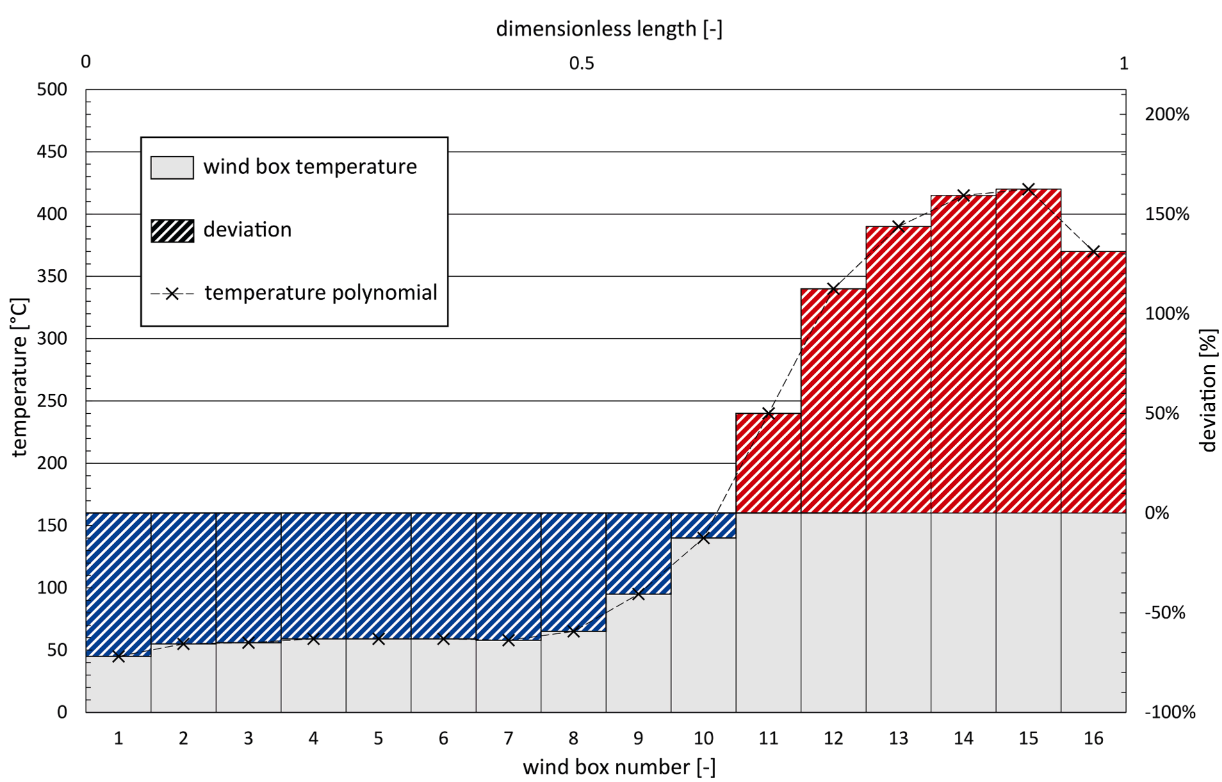

Fig. 6. Schematic of the wind box temperature calculation with a $T_{off-gas}$ of 160°C.

operation of the plant without SWGR and operation of the plant with SWGR. Both simulation scenarios had a mainly feed-forward oriented calculation structure. The number of wind boxes, and the wind boxes used for waste gas recirculation, were based on the publication by Schmid et al. [29]. The gas flows of wind boxes 11 to 16 were recirculated at the SWGR scenario. Both scenarios had the same sinter strand length, sinter production, total off-gas volume to produced sinter ratio, and conversion rates. Furthermore, the carbon monoxide and sulfur dioxide concentration of the stack gas flow and the temperature ratio of the last wind box to the sinter outlet were considered equal in both scenarios. The wind box temperatures' distribution functions were based on plant data with SWGR and without SWGR. All input streams were kept constant. Only one single coke stream was adjusted in the scenario without SWGR for ensuring comparable process temperatures in both scenarios.

3.1. Validation of Simulation Results

To show the validity of the selected operational settings, the SWGR was introduced in an iron ore sinter plant. The simulated stack gas characteristics are compared with stack gas measurements of a sinter plant before and after its SWGR introduction. The measured data show a significant variation of the stack gas flow compared to its average value. The calculated volumetric flow of the SWGR scenario is in the range of plant data. The temperature measurements of the stack gas show that the average stack gas temperature at a sinter strand with SWGR is 21°C higher than a sinter strand without SWGR. The difference can be explained by the different inlet temperatures of the process gas in both scenarios. Fig. 7 shows that the simulation results are in the range of measured plant data.

3.2. Main Solid and Gas Streams

Fig. 8 shows all solid and liquid input and output streams of the sinter plant model.The sinter production remains constant, corresponding to the scenario settings. This leads to the same input streams of iron carrier and additives in both scenarios. However, the resulting solid fuel and water streams are noticeably different. In the SWGR scenario, the coke consumption is reduced by 11% compared to the scenario without SWGR. These results are within the observed plant data range (8–13%) [29,31]. There are two reasons for this effect: (1) By recycling carbon monoxide and its partly exothermic oxidization to carbon dioxide, more heat is generated during the sintering process. (2) By mixing fresh air with the recycle stream in the SWGR scenario, the process gas stream attained a higher temperature than the scenario without SWGR, which uses only fresh air. Therefore, less energy is necessary to enable the required process temperatures and, consequently, the coke amount declines. An unexpected side effect is that more water needs to be added to the granulator to enable the same water ratio in the raw mixture in both scenarios due to coke's natural water content. Caused by the reduced coke input, the required water increases by 3.2% in the SWGR scenario compared to the scenario without SWGR.

Fig. 9 compares gaseous input and output streams based on the assumption of a constant ratio of total off-gas to produced sinter for the scenario with SWGR and without SWGR. Process air is the summation of fresh air, recycled gas, and combustion gases from the ignition hood. In the scenario without SWGR, the amount of fresh air and process air are identical because no gas stream is recirculated from the wind boxes. In the scenario with SWGR, the fresh air consumption is decreased because process air contains the recirculated gas stream and fresh air.

The total process air consumption is similar in both scenarios based on the defined constant mole-based ratio of total off-gas to produced sinter. The slight mass flow difference is based on changing process air composition.

Combining recycle gas with fresh air results in a oxygen and water vapour content of 19.5 % and 1.3 %. Oxygen content is in a reasonable range of 19–20 % as given by literature [21,32,33]. Due to the same sinter production rate and similar amounts of process gas in both cases, the off-gas is similar as well. However, splitting the off-gas stream in case of introduced SWGR into recycle flow and stack flow reduces the stack gas flow compared to the scenario without SWGR.

Fig. 10 shows the change of total component flows of the SWGR scenario based on the scenario without SWGR in the stack gas. The introduction of SWGR affects each component flow in the off-gas stream differently. The flow change of nitrogen correlates to the amounts of fresh air in both scenarios and decreases in the same ratio. In the SWGR case, the much lower oxygen flow can be explained by reducing fresh air and using recycled oxygen for carbon and carbon monoxide oxidation.

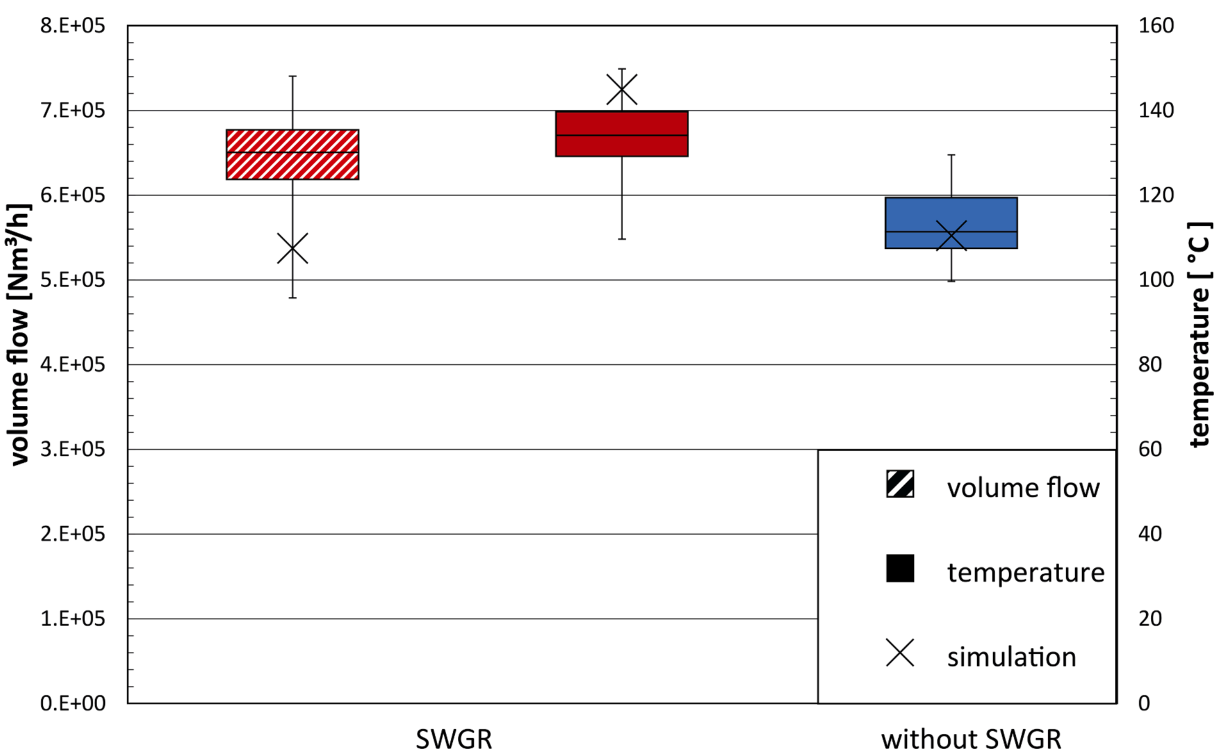

Fig. 7. Comparision stack gas measurements with simulation results.

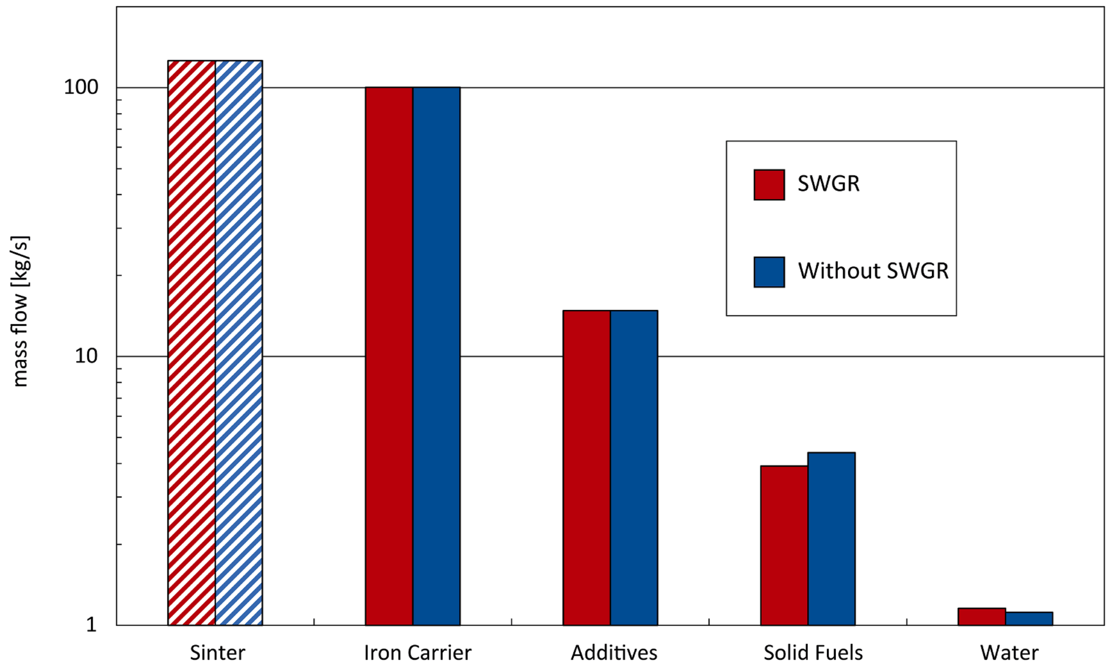

Fig. 8. Comparison of solid input (plain) and output (hatched) streams.

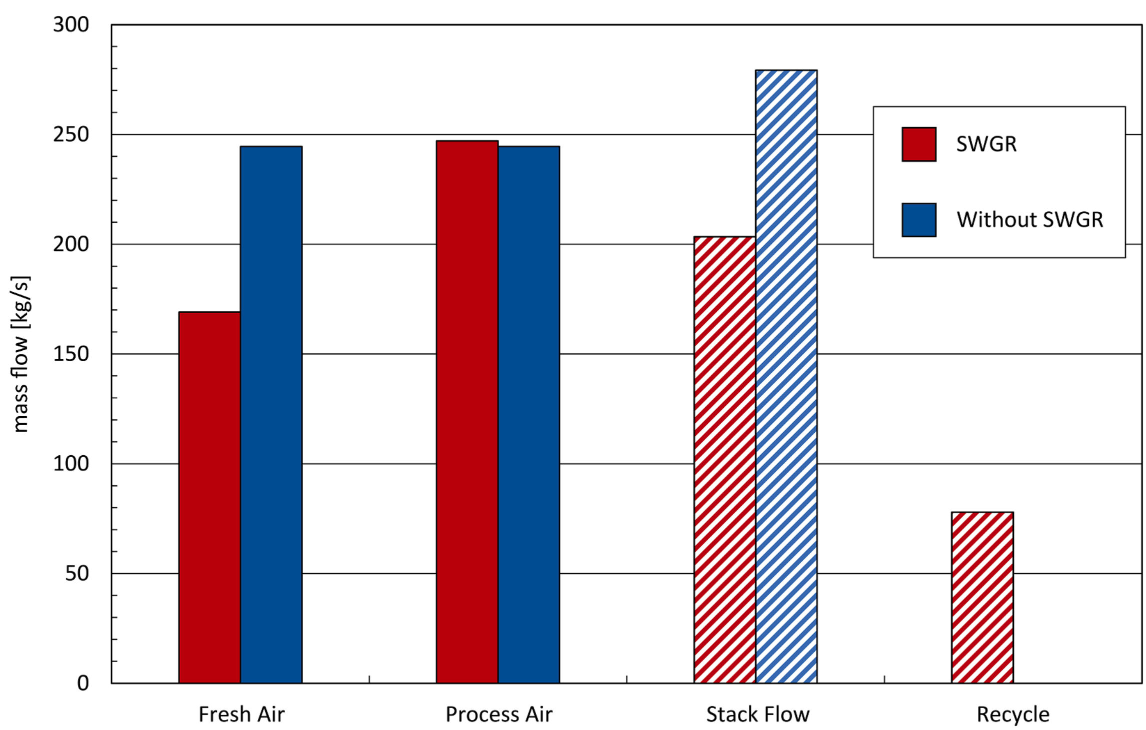

Fig. 9. Comparison of gaseous input (plain) and output (hatched) streams.

Surprisingly, in the stack-gas, the flow rate of CO_2 is slightly higher, although the coke demand is reduced at the SWGR scenario. Both scenarios have similar production rates and produce the same amount of carbon dioxide during carbonate decomposition. However, in the SWGR scenario, the entering carbon monoxide of the recycling is oxidized mainly to carbon dioxide, which explains the higher CO_2 flow in the SWGR scenario than in the scenario without SWGR. In sub-chapter 3.4 the carbon dioxide flow is described in more detail. The carbon monoxide and sulfur flows decrease at the same ratio as the stack gas since constant carbon monoxide and sulfur dioxide concentrations of the stack gas are assumed for the calculation based on observations from a sinter plant. In the SWGR scenario, the lower coke input stream has a minor influence on the sulfur dioxide reduction because the sulfur input mainly originates from iron and additive sources. The reduced sulfur content in the stack gas at unchanged sulfur inputs in the SWGR scenario is explained by higher sulfur binding in the sinter, considered by an empirical factor implemented in the simulation model. This behavior is shown in more detail in Fig. 14. The nearly similar water vapor flows in the stack gas are based on similar water inputs in the raw mixtures. The lower coke consumption in the SWGR scenario lowers the water content,

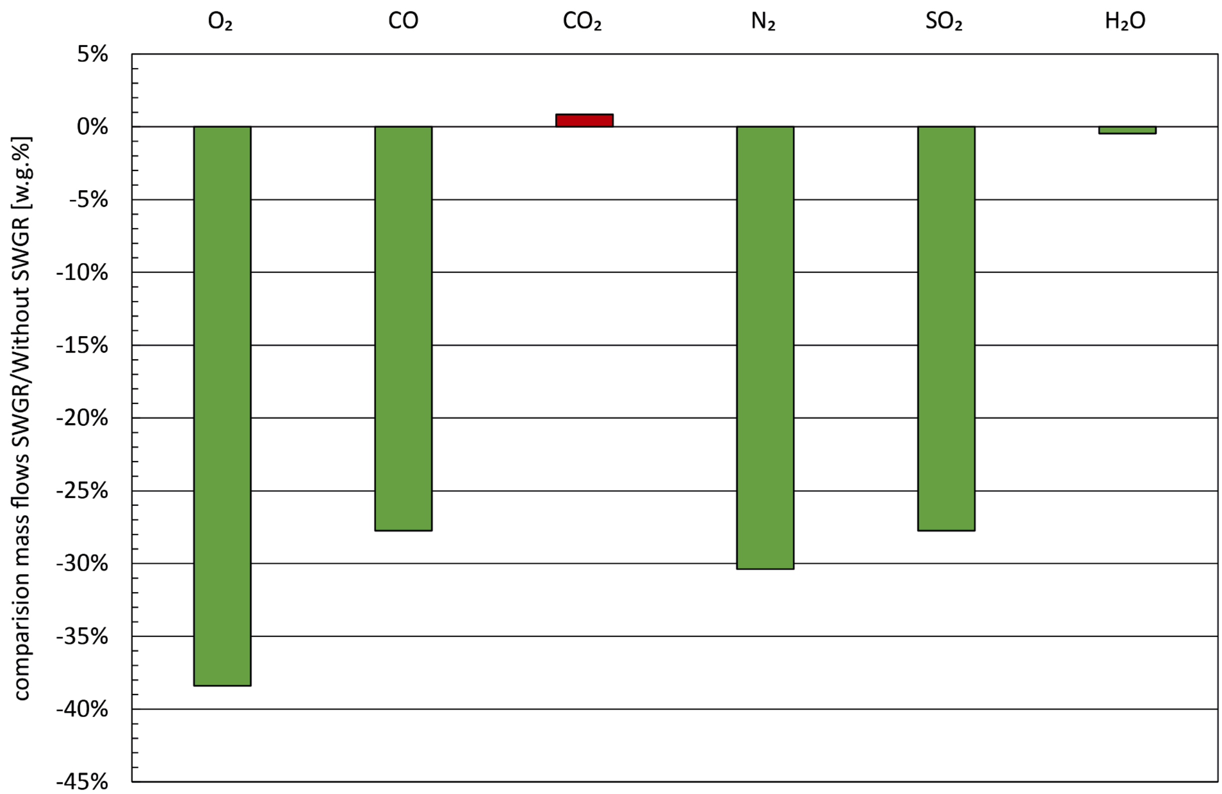

Fig. 10. Comparison of main component flows in stack-gas.

but the granulator compensates this effect. During the granulation, water is added to achieve the same water ratio in the raw mixture as in the scenario without SWGR.

3.3. Oxygen Conversion

Fig. 11 shows the oxygen balance of the black-box model. Comparing the results from Fig. 11 and Fig. 9, the oxygen flow and the airflow are reduced at the same ratio in the SWGR scenario. About 75 % of the total

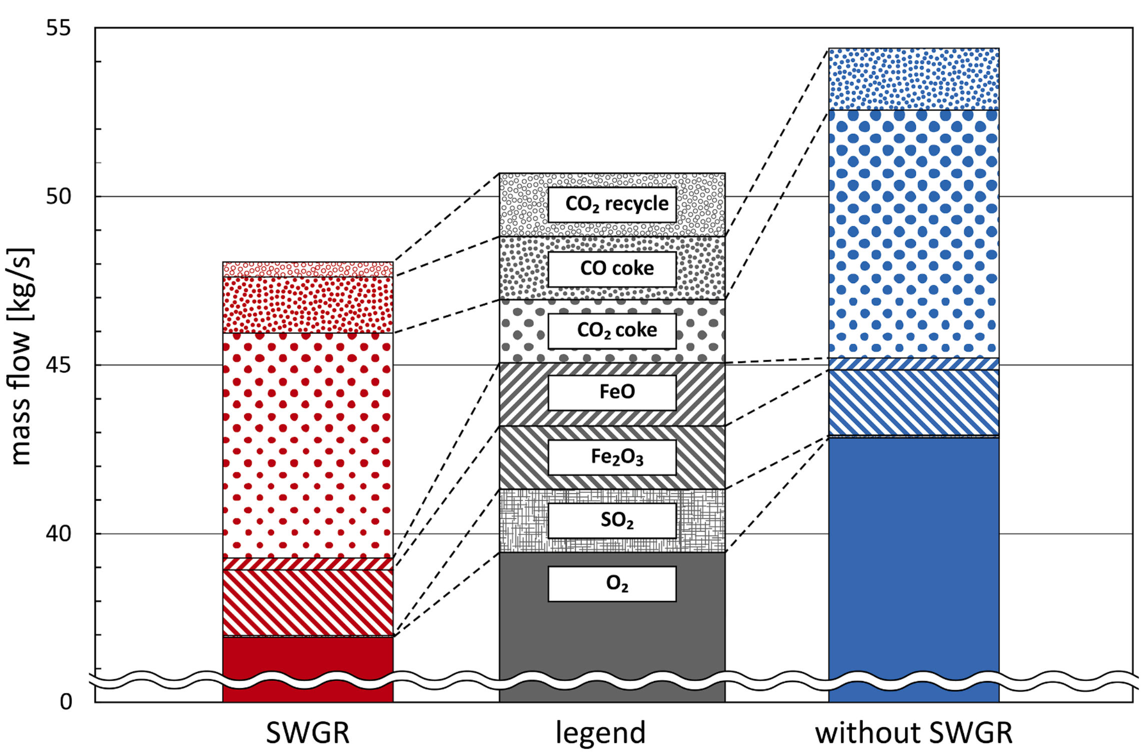

Fig. 11. Oxygen balance of black-box.

oxygen flow are not reacting with other components. Conversions with carbon are the most oxygen-consuming reactions. Most carbon is directly oxidized to carbon dioxide, followed by the conversion to carbon monoxide. In the SWGR scenario, the oxidation of the recycled carbon monoxide is noticeable. Iron oxidations are the second most oxygen-consuming reactions. In our scenarios, most iron ores are oxidized to Fe_2O_3 and secondly to FeO. The sulfur reaction of oxygen-consuming and oxygen-releasing reactions are summarized in Fig. 11 with the label sulfur dioxide. For the scope of produced emissions and for environmental impacts, the sulfur conversion is a crucial issue, but it hardly affects the oxygen balance. In the scenario without SWGR, no part of the off-gas is recycled. Based on the model design, the recycled carbon monoxide oxidation and the sulfur binding are not occurring in this case. These effects are discussed in more detail in the sub-chapters 3.5 and 3.6.

3.4. Carbon Dioxide Conversion

Fig. 12 compares the CO_2 origin of both scenarios. In both cases, additives are the main carbon dioxide source. They account for around two-thirds of the total carbon dioxide flow. The second-largest CO_2 source originates from coke combustion. The third and smallest CO_2 source arises from recycled CO oxidation. In contrast to the oxidation of recycled CO, the declining coke consumption has a minor influence on the CO_2 stream in the SWGR scenario. Consequently, the mass flow of carbon dioxide is slightly higher in scenario with SWGR compared to the scenario without SWGR.

3.5. Carbon Monoxide Conversion

Fig. 13 shows the origin of the carbon monoxide flow in the off-gas stream. In the scenario without SWGR, no carbon monoxide is recirculated to the sinter strand. Therefore, carbon monoxide originates only from coke sources. In the scenario with SWGR, carbon monoxide results from solid fuels and the remaining carbon monoxide of the recycle stream, which is not oxidized to carbon dioxide, shown in red scattered style on the top of the SWGR bar (Fig. 13).

3.6. Sulfur Conversion

About three-fourths of the sulfur input originates from iron carrier input streams. These material flows contain iron ores and byproducts from several processing operations of integrated steelworks (e.g.casting, rolling mill). Solid fuels are the second important source of sulfur by about 24% (scenario without SWGR). Only 2% of the total sulfur feedstock originates from additive sources.

As shown in Fig. 14, in the SWGR scenario, sulfur dioxide emissions are reduced by 27%. In contrast, the sulfur content of the sinter is doubled due to sulfur dioxide binding by the sinter considered in the model with an empiric factor. Reduction of coke demand only contributes to minor part to the reduction of sinter emissions since the sulfur input is reduced only by 2.5%.

3.7. Chlorine Balance

As shown in Fig. 15, most of the chlorine originates from iron carrier input streams by 90%. The amount of chlorine from coke and additive lies only at 4% and 6%, respectively. The changing coke consumption declines the total chlorine input amount only by 1%. It has a minor influence on the chlorine balance. About 15% of total chlorine feedstock is leaving the sinter plant via the solid sinter. The other 85% of the chlorine input leaves the sinter plant by stack-gas.

4. Conclusion

The scenarios calculated with SWGR and without SWGR shows that the sinter model provides reliable results compared to observed plant data and known effects. The simulated stack temperatures are within a realistic temperature range. Under SWGR conditions, the model shows an credible reduction of coke consumption, stack gas, and sulfur dioxide

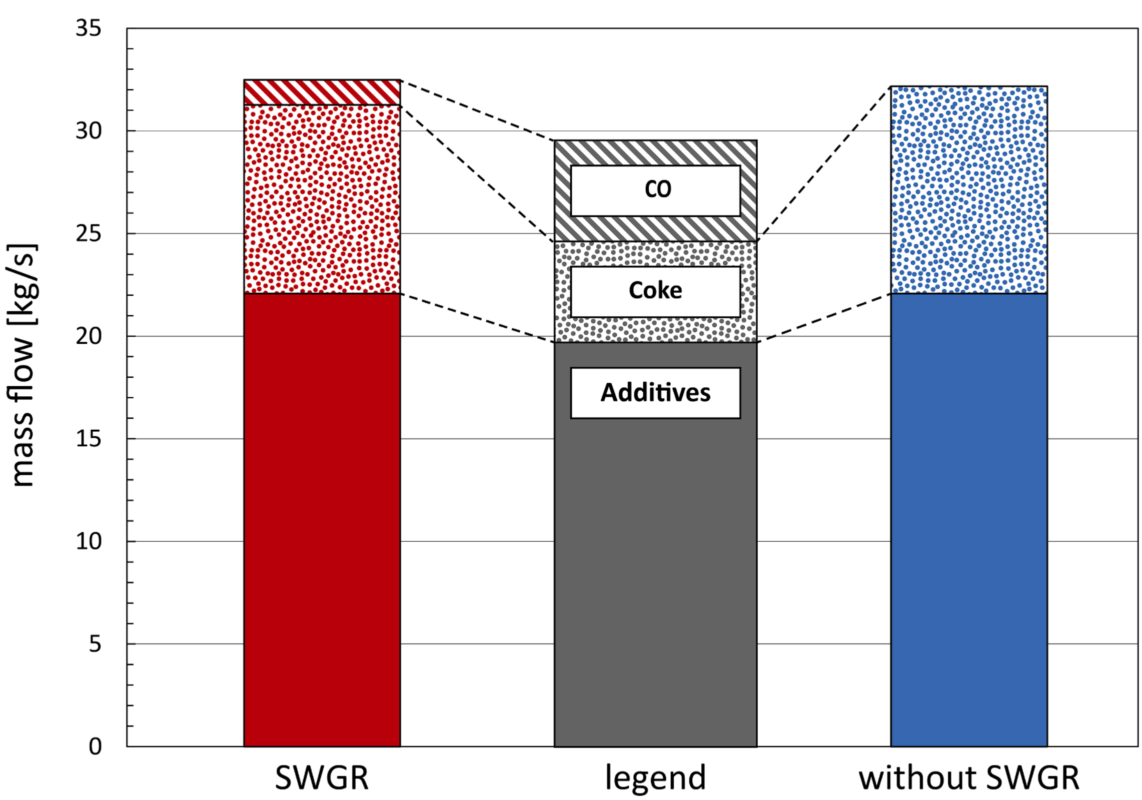

Fig. 12. Origin of CO_2 in off-gas.

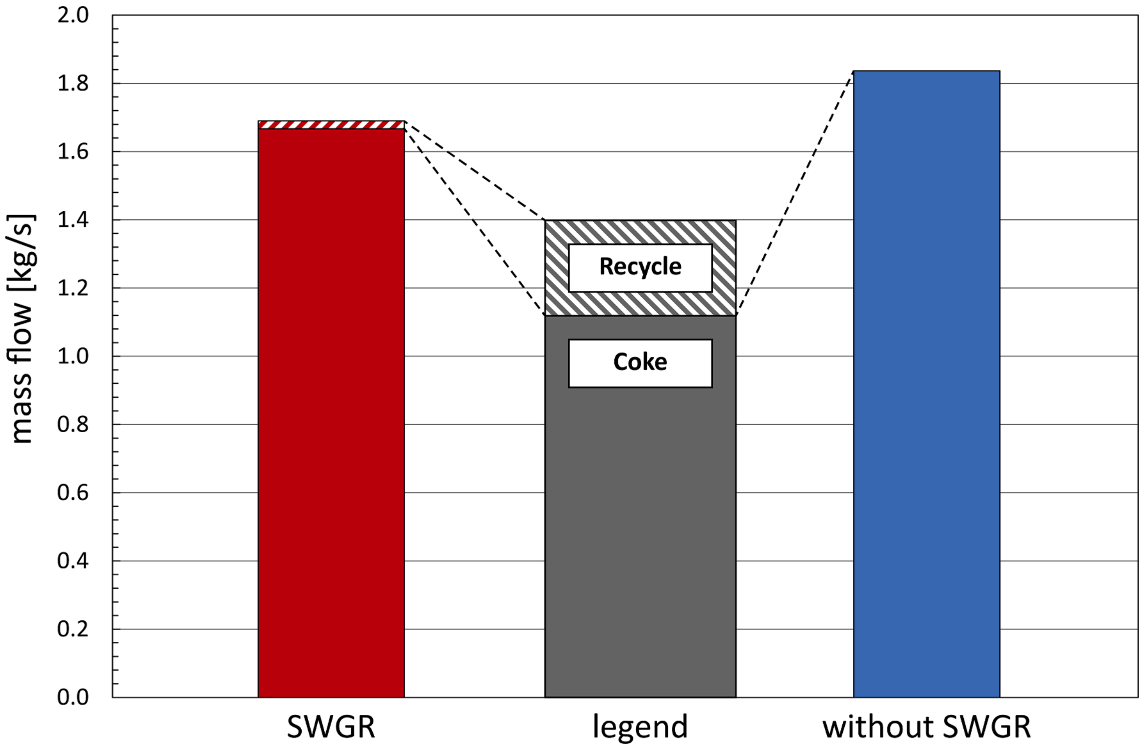

Fig. 13. Origin of carbon monoxide in off-gas.

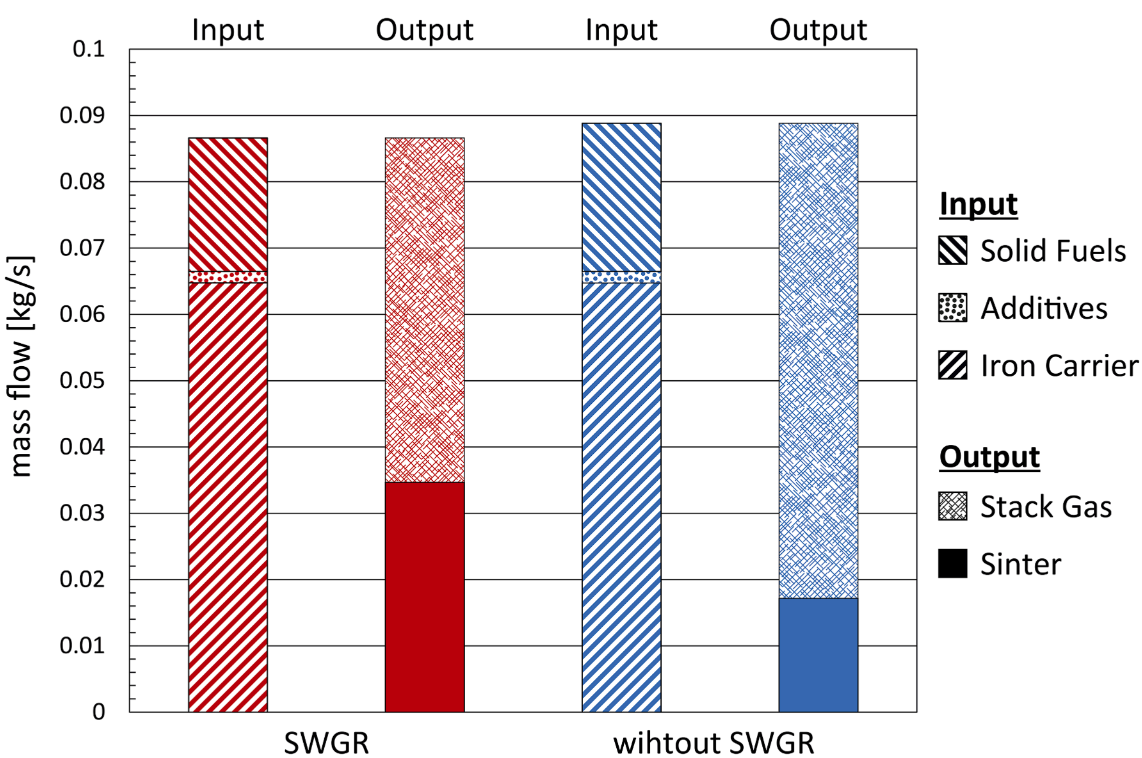

Fig. 14. Sulfur balance of solid input and output streams.

emissions by 11%, 27%, and 27%. In contrast, in the SWGR scenario, the total stack gas flow of carbon dioxide is higher than in the scenario without SWGR. This effect correlates with the oxidation of the recycled carbon monoxide. Two-thirds of the produced carbon dioxide originates from thermal carbonate decomposition processes. Most of the converted oxygen is used for carbon oxidation and iron oxidation.

For the SWGR scenario, the model correctly considers the effect of reduced sulfur dioxide emissions with the stack due to the sulfur binding. The coal reduction has just a minor effect. Under SWGR conditions, the sinter model shows only a low reduction potential of chlorine emissions.

In the future a correlation between temperature distribution and

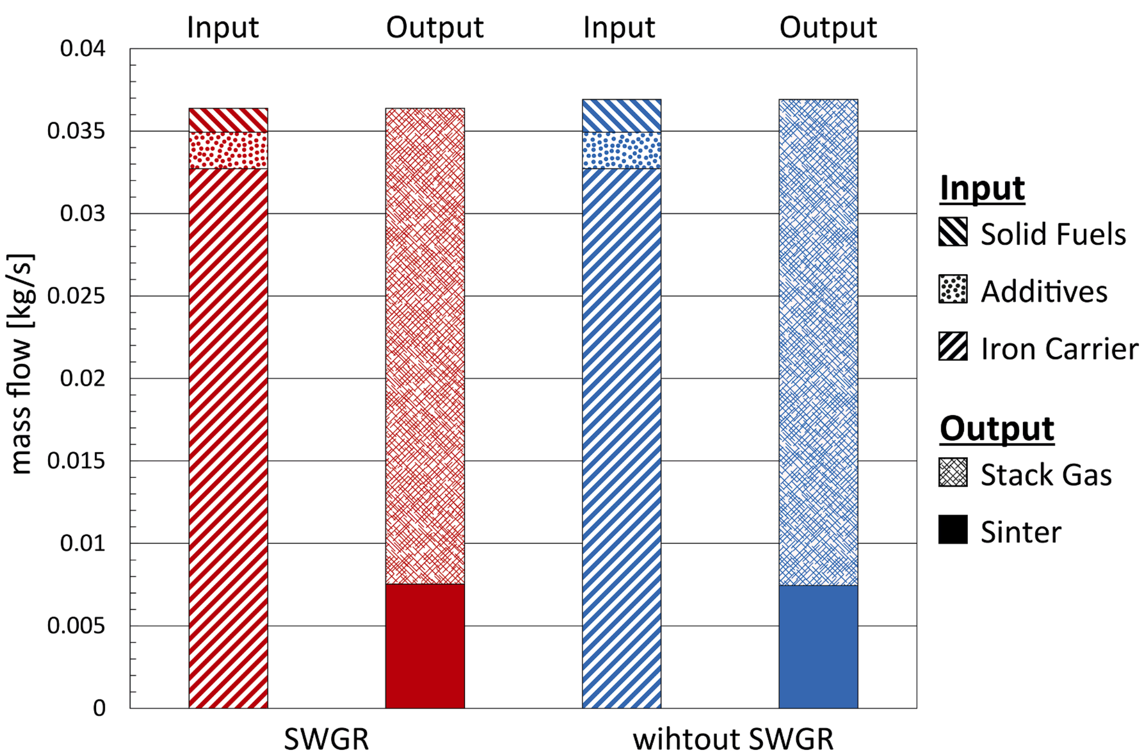

Fig. 15. Chlorine balance of solid input and output streams.

mass distribution will be implemented to the sinter plant model. A changing temperature function will adjust the influence the mass distribution function. Additional studies on trace element sources and reactions are recommended for improving the sinter model's prediction capabilities.

CRediT authorship contribution statement

Johannes Niel: Visualization, Writing - original draft, Data curation, Investigation, Formal analysis, Validation, Software, Conceptualization, Methodology. **Bernd Weiss:** Project administration, Writing - review & editing, Software, Conceptualization. **Walter Wukovits:** Software, Project administration, Writing - review & editing, Resources, Conceptualization.

Declaration of Competing Interest

The authors declare that they have no known competing financial interests or personal relationships that could have appeared to influence the work reported in this paper.

Acknowledgements

The authors gratefully acknowledge the funding of work by the research program COMET (Competence Center for Excellent Technologies), the Austrian program for competence centers (FFG contract number 869295), and the support of Bernhard Rummer (Voestalpine Stahl Linz GmbH) and Herbert Schmid (Voestalpine Stahl Linz GmbH) by providing plant data and their expertise.

References

[1] F. Cappel, H. Wendeborn, Sintern von Eisenerzen, Vol. 19, Stahleisen M.B.H, Düsseldorf, 1973.
[2] O. Almpanis-Lekkas, Model development of metallurgical unit operations for use in a process simulation tool, Technische Universität Wien, Wien, 2015.
[3] F. Cappel, Wärmebehandlung des Sinters mit heißen Rauch- oder Prozeßgasen im Anschluß an den Zündofen, RWTH Aachen, Aachen, 1977.
[4] O. Almpanis-Lekkas, M. Mühlböck, B. Weiss, W. Wukovits, Model development of sinter plant with feasible selective waste gas recirculation 11 (11) (2015) 162–165.
[5] W. Yang, S. Choi, E.S. Choi, D.W. Ri, S. Kim, Combustion characteristics in an iron ore sintering bed—evaluation of fuel substitution, Combustion and Flame 145 (3) (2006) 447–463, https://doi.org/10.1016/j.combustflame.2006.01.005.
[6] H. Ahn, S. Choi, B. Cho, Process simulation of iron ore sintering bed with flue gas recirculation, Ironmaking & Steelmaking 40 (2) (2013) 120–127, https://doi.org/10.1179/1743281212Y.0000000071.
[7] J. Mitterlehner, G. Loeffler, F. Winter, H. Hofbauer, H. Schmid, E. Zwittag, T. H. Buergler, O. Pammer, H. Stiasny, Modeling and simulation of heat front propagation in the iron ore sintering process, ISIJ International 44 (1) (2004) 11–20, https://doi.org/10.2355/isijinternational.44.11.
[8] M. Kenny, T. Oates, Lime and limestone, in, Ullmann's encyclopedia of industrial chemistry, Vol. 47, Wiley, Chichester, 2010, p. 2443, 10.1002/14356007.a15_317.pub2.
[9] L. Wang, Y.-H. Li, J.-L. Lu, W. Xu, H.-L. Lin, Thermal decomposition kinetics of manganese carbonate in the process of mnzn ferrite preparation, in: TMS (Ed.), TMS 2016: 145th Annual Meeting & Exhibition: Supplemental Proceedings, Vol. 34, John Wiley & Sons Inc, Hoboken, NJ, USA, 2016, pp. 335–342. doi:10.1002/9781119274896.ch40.
[10] S. Maitra, N. Bandyopadhyay, S. Das, A.J. Pal, J. Pramanik, Non-isothermal decomposition kinetics of alkaline earth metal carbonates, Journal of the American Ceramic Society 90 (4) (2007) 1299–1303, https://doi.org/10.1111/j.1551-2916.2007.01607.x.
[11] Y. Tang, M. Chu, J. Tang, L. You, Z. Liu, The oxidation and decomposition behavior of carbonate iron ore, Steel Research International 88 (2) (2017) 1600129, https://doi.org/10.1002/srin.201600129.
[12] W. Yang, C. Ryu, S. Choi, E. Choi, D. Lee, W. Huh, Modeling of combustion and heat transfer in an iron ore sintering bed with considerations of multiple solid phases, ISIJ International 44 (3) (2004) 492–499, https://doi.org/10.2355/isijinternational.44.492.
[13] N.K. Nath, A.J. da Silva, N. Chakraborti, Dynamic process modelling of iron ore sintering, Steel Research 68 (7) (1997) 285–292, https://doi.org/10.1002/srin.199701791.
[14] N.K. Nath, K. Mitra, Mathematical modeling and optimization of two-layer sintering process for sinter quality and fuel efficiency using genetic algorithm, Materials and Manufacturing Processes 20 (3) (2005) 335–349, https://doi.org/10.1081/AMP-200053418.
[15] O. Rentz, M. Fröhlich, F. Nebel, F. Schultmann, B. Engels, Integrierter Umweltschutz in der Metallerzeugung Simulationsgestützte operative Produktionsplanung zur Optimierung metallurgischer Abfallverwertungsprozesse, Schlussbericht (2005).
[16] W. Yang, C. Ryu, S. Choi, E. Choi, D.W. Ri, W. Huh, Mathematical model of thermal processes in an iron ore sintering bed, Metals and Materials International 10 (5) (2004) 493–500, https://doi.org/10.1007/BF03027355.

[17] I. Muchi, J. Higuchi, Theoretical analysis on the operation of sintering, Tetsu-to-Hagane 56 (3) (1970) 371–381, https://doi.org/10.2355/tetsutohagane1955.56.3_371.

[18] J.A. d. Castro, Y. Sazaki, J.-I. Yagi, Three dimensional mathematical model of the iron ore sintering process based on multiphase theory, Materials Research 15 (6) (2012) 848–858. doi:10.1590/S1516-14392012005000107.

[19] J.A. d. Castro, J.L. Pereira, V.S. Guilherme, E.P. da Rocha, A.B. França, Model predictions of pcdd and pcdf emissions on the iron ore sintering process based on alternative gaseous fuels, Journal of Materials Research and Technology 2 (4) (2013) 323–331. doi:10.1016/j.jmrt.2013.06.002.

[20] M.V. Ramos, E. Kasai, J. Kano, T. Nakamura, Numerical simulation model of the iron ore sintering process directly describing the agglomeration phenomenon of granules in the packed bed, ISIJ International 40 (5) (2000) 448–454, https://doi.org/10.2355/isijinternational.40.448.

[21] S. Zhang, Z. Wen, G. Wang, R. Dou, X. liu, X. Li, The effects of operational parameters on flue gas recirculation iron ore sintering process: sensitivity analysis based on numerical simulation and industrial onsite experimental validation, Ironmaking & Steelmaking, 47 (4) (2020) 368–380. doi:10.1080/03019233.2018.1521565.

[22] N. Oyama, Y. Iwami, T. Yamamoto, S. Machida, T. Higuchi, H. Sato, M. Sato, K. Takeda, Y. Watanabe, M. Shimizu, K. Nishioka, Development of Secondary-fuel Injection Technology for Energy Reduction in Iron Ore Sintering Process, Tetsu-to-Hagane 97 (10) (2011) 510–518, https://doi.org/10.2355/tetsutohagane.97.510.

[23] Z. Cheng, J. Wang, S. Wei, Z. Guo, J. Yang, Q. Wang, Optimization of gaseous fuel injection for saving energy consumption and improving imbalance of heat distribution in iron ore sintering, Applied Energy 207 (2017) 230–242, https://doi.org/10.1016/j.apenergy.2017.06.024.

[24] Z. Cheng, J. Wang, S. Wei, Z. Guo, J. Yang, Q. Wang, Improvement of heat pattern and sinter strength at high charcoal proportion by applying ultra-lean gaseous fuel injection in iron ore sintering process, Journal of Cleaner Production 161 (2017) 1374–1384, https://doi.org/10.1016/j.apenergy.2017.06.024.

[25] X. Huang, X. Fan, Z. Ji, M. Gan, X. Chen, Y. Zhao, T. Jiang, Investigation into the characteristics of H2-rich gas injection over iron ore sintering process: Experiment and modelling, Applied Thermal Engineering 157 (78) (2019), 113709, https://doi.org/10.1016/j.applthermaleng.2019.04.119.

[26] W. Ni, H. Li, L. Shao, Z. Zou, Numerical Simulation on Influence of Coke Oven Gas Injection on Iron Ore Sintering, ISIJ International 60 (4) (2020) 662–673, https://doi.org/10.2355/isijinternational.ISIJINT-2019-486.

[27] N. Tsioutsios, C. Weiß, J. Rieger, E. Schuster, B. Geier, Flame front progress in gas assisted iron ore sintering, Applied Thermal Engineering 165 (9) (2020), 114554, https://doi.org/10.1016/j.applthermaleng.2019.114554.

[28] H.D. Baehr, S. Kabelac, Thermodynamik: Grundlagen und technische Anwendungen, 14th Edition,, Springer-Lehrbuch, Springer-Verlag Berlin Heidelberg, Berlin, Heidelberg, 2009, 10.1007/978-3-642-00556-5.

[29] H. Schmid, W. Ehler, E. Zwittag, Operational experience with the new eposint gas recycling process at sinter strand no 5 of voestalpine stahl in linz, Proceedings/ 3rd International Steel Conference on New Developments in Metallurgical Process Technologies 3 (2007) 331–338.

[30] G. Brunnbauer, W. Ehler, E. Zwittag, H. Schmid, J. Reidetschläger, K. Kainz, Eposint- ein neues konzept zur abgasrückführung für sinteranlagen, Stahl und Eisen 126 (9) (2006) 41–46.

[31] J. Reidetschläger, H. Stiasny, S. Hötzinger, C. Aichinger, A. Fulgencio, Siemens vai sintering selective waste gas recirculation system: Meet the future's environmental requirements today, Iron and Steel Technology 7 (3) (2010) 54–59.

[32] X-h. Fan, Z-y. Yu, M. Gan, W-q. Li, Z-y. Ji, Influence of O2 Content in Circulating Flue Gas on Iron Ore Sintering Journal of Iron and Steel Research International, 20 (1) (2013) 1–6. doi:10.1016/S1006-706X(13)60103-X.

[33] X-h. Fan, Z-y. Yu, M. Gan, W-q. Li, Z-y. Ji, Establishment of refined sintering flue gas recirculation patterns for gas pollutant reduction and waste heat recycling, Journal of Cleaner Production 235 (2019) 1549–1558, https://doi.org/10.1016/j.jclepro.2019.07.003.